Numerical investigation of extensional flow through axisymmetric conical geometries: Finite element method

Ahmed N. Abdulhasan , Alaa H. Al-Muslimawi*

Department of Mathematics, College of Sciences, University of Basrah, Basra, Iraq.

*Corresponding author, E-mail: alaamath73@gmail.com

Doi 10.29072/basjs.202033

Abstract

In this article, we present the numerical investigation for incompressible Newtonian laminar flow through a conical channel. We apply the Galerkin finite element method for solving the governing equations of such a problem. Usually, the governing equations for incompressible Newtonian flows are represented by conservation laws for mass and momentum, which are given in the cylindrical coordinates (axisymmetric) in the current study. Interestingly, the pressure drop through the channel is provided under a variety of Reynolds numbers. The objective of this study is to assess the influence of various effective parameters on the level of the pressure drop. Further, the effect of the boundary maximum axial velocity that is imposed at the inlet upon the solution reveals some novel features. To evaluate the influence of the conical half-angle at the recirculation region on solutions behavior, this study is achieved with a different set of angles. We found that the conical half-angle was notably affecting the critical level of pressure drop. Moreover, the response of the fluid in both shear and extensional is quite interesting, which represents one of the more important aspects of this study.

Article inf.

Received: 1/12/2020

Accepted

22/12/2020

Published

31/12/2020

Keywords:

Conical flow, Finite element method, Galerkin method, Navier-Stokes equations, Newtonian fluid

1. Introduction

A numerical investigation of incompressible Newtonian fluid flow through a conical channel is introduced in the present study. Navier-Stokes equations are the partial differential equations that describe the fluid flow phenomena. For Newtonian fluids, the relation between the stress tensor and the rate of deformation tensor can be expressed by a linear relation, while that does not hold for non-Newtonian fluids [1–3]. This linear relation is considered as the simplest relationship that describes the relationship between these tensors. Furthermore, the flow is selected to be laminar and isothermal. In laminar flow, the fluid moves and travels smoothly in the channel. Various studies of the solution for incompressible Newtonian equations have been occurred in literature (for example see: [1,4–6]). Geometrically, the flow channel is selected to have a converging mid-section to satisfy some desired results.

The converging flow may be introduced as a geometrical concept mediates in-between the uniform and sudden contraction flow [7]. The conical flow can be defined as a uniform flow with a section of gradual contraction. The axisymmetric conical channel is considered in the present study, it is selected as its wide-spreading in the practical fields. The conical flow is classified as one of the essential internal flows. Many accomplished types of research include converging flow had been published (see for example: [8–12]). Mostly, the objective of the converging flow studies is to give an essential understanding or to expand an experimental basis so the empirical predictions can be done [13]. The characteristics of the geometry have a huge effect on the flow characteristics. The geometric parameters of the conical flow: the half-angle (α), the ratio between the length to the diameter of the upstream section, and the ratio between upstream to downstream diameters are considered as characteristics of the conical geometry [14,15]. Under normal circumstances, the geometric parameters varying leads to a significant impact on mass flow rate [15]. Also, changes in the static pressure and drag force are correlated to the changes of geometric parameters [15]. In the conical flow, the flow generates regions of near-sink flow for specific sets of Reynolds numbers [16,17].

In this study, a numerical simulation based on Galerkin finite element method is achieved to treat incompressible Newtonian flow through an axisymmetric conical channel. The novelty in this study the temporal convergence-rate of the system solution that is taken to be steady-state and the effect of many factors on such a problem with a new geometry pattern, which did not address by researchers previously. In this context, Poiseuille (*PS*) flow along a two-dimensional axisymmetric conical channel, under isothermal conditions is studied. The main results of the current study focus on the convergence rate of velocity and pressure solutions. The relationship between pressure and Reynolds number is shown as well. The effect of boundary maximum axial velocity ($(u_z)_{max}$) at the inlet of the channel on the level of *Re* is also investigated. Also, the impact of varying conical half-angle on pressure drop and flow velocity is considered. The fluid response under shear and extensional deformation conditions is considered. In this context, the effect of Reynolds number and conical half-angle on stress response is studied.

In the next section, the mathematical modeling of the motion of the Newtonian flows will be presented. These equations are introduced in the cylindrical coordinates. Since these equations must be studied numerically, the numerical method will be characterized in section 3. The problem discretization and the related numerical results will be explained in sections 4 and 5, respectively.

2. Mathematical modeling

The system of the differential equation that governs the incompressible Newtonian flow consists of two essential equations: continuity equation and momentum equation [3,18]. The dimensionless form with omitted body forces of the balance equations under isothermal conditions may be expressed as [3,19]:

$$\nabla . u = 0 \tag{1}$$

$$\frac{\partial u}{\partial t} + u.\nabla u = -\frac{1}{Re}\nabla p + \frac{1}{Re}\nabla^2 u, \tag{2}$$

where, u is the velocity vector, p is the pressure, and $Re = \rho UL/\mu$ is the Reynolds number [3,20–22], where, ρ is the fluid density, L is the scale length, and U is the scaled velocity. In the cylindrical coordinates, the incompressible equations (1)-(2) are given in the components form as [19,23–26]:

$$\frac{1}{r}\frac{\partial}{\partial r}(ru_r)+\frac{1}{r}\frac{\partial u_\theta}{\partial \theta}+\frac{\partial u_z}{\partial z}=0 \tag{3}$$

r-direction

$$\frac{\partial u_r}{\partial t}+u_r\frac{\partial u_r}{\partial r}+\frac{u_\theta}{r}\frac{\partial u_r}{\partial \theta}+u_z\frac{\partial u_r}{\partial z}-\frac{u_\theta^2}{r}= -\frac{1}{Re}\frac{\partial p}{\partial r}+\frac{1}{Re}\left[\frac{\partial}{\partial r}\left(\frac{1}{r}\frac{\partial}{\partial r}(ru_r)\right)+\right.$$
$$\left.\frac{1}{r^2}\frac{\partial^2 u_r}{\partial \theta^2}+\frac{\partial^2 u_r}{\partial z^2}-\frac{2}{r^2}\frac{\partial u_\theta}{\partial \theta}\right], \tag{4}$$

θ-direction

$$\frac{\partial u_\theta}{\partial t}+u_r\frac{\partial u_\theta}{\partial r}+\frac{u_\theta}{r}\frac{\partial u_\theta}{\partial \theta}+u_z\frac{\partial u_\theta}{\partial z}+\frac{u_r u_\theta}{r}=-\frac{1}{r}\frac{1}{Re}\frac{\partial p}{\partial \theta}+\frac{1}{Re}\left[\frac{\partial}{\partial r}\left(\frac{1}{r}\frac{\partial}{\partial r}(ru_\theta)\right)+\right.$$
$$\left.\frac{1}{r^2}\frac{\partial^2 u_\theta}{\partial \theta^2}+\frac{\partial^2 u_\theta}{\partial z^2}+\frac{2}{r^2}\frac{\partial u_r}{\partial \theta}\right], \tag{5}$$

z-direction

$$(6)\quad \frac{\partial u_z}{\partial t}+u_r\frac{\partial u_z}{\partial r}+\frac{u_\theta}{r}\frac{\partial u_z}{\partial \theta}+u_z\frac{\partial u_z}{\partial z}=-\frac{1}{Re}\frac{\partial p}{\partial z}+\frac{1}{Re}\left[\frac{1}{r}\frac{\partial}{\partial r}\left(r\frac{\partial u_r}{\partial r}\right)+\frac{1}{r^2}\frac{\partial^2 u_z}{\partial \theta^2}+\frac{\partial^2 u_z}{\partial z^2}\right].$$

3. Numerical method

To solve the related governing equations (3)-(6), Galerkin finite element method (GFEM) is utilized. The starting point of this approach is to find the weak form of the equation by using appropriate weight functions. Firstly, by multiplying via appropriate weight functions for both: continuity and momentum equations, integrating over a typical domain; and substituting assumed approximate solutions, so the matrix form of these equations is given by:

$$[T][\dot{U}_r]+([Q]+[T_a])[U_r]+([S_\theta(U_\theta)]+[D_\theta])[U_\theta]-\frac{1}{Re}[F_r][P]=[0], \tag{7}$$

$$[T][\dot{U}_\theta]-[D_\theta][U_r]+([Q]+[T_a]+[S_r(U_r)])[U_\theta]-\frac{1}{Re}[F_\theta][P]=[0], \tag{8}$$

$$[T][\dot{U}_z]+[Q][U_z]-\frac{1}{Re}[F_z][P]=[0], \tag{9}$$

$$([F_r^T]+[F_a])[U_r]+[F_\theta^T][U_\theta]+[F_z^T][U_z]=[0], \tag{10}$$

where, $[Q] = [Y_r(U_r)] + [Y_\theta(U_\theta)] + [Y_z(U_z)] + [H_r] + [H_\theta] + [H_z] + [D_r]$, and U_r, U_θ, U_z, and P are coefficients which are found by the assumed approximate solutions. The quadratic shape functions that are proposed for velocity components are defined as:

$$\begin{bmatrix}\psi_1\\\psi_2\\\psi_3\\\psi_4\\\psi_5\\\psi_6\end{bmatrix} = \begin{bmatrix}L_1^2 - L_1L_2 - L_1L_3\\L_2^2 - L_2L_3 - L_2L_1\\L_3^2 - L_3L_1 - L_3L_2\\4L_1L_2\\4L_2L_3\\4L_3L_1\end{bmatrix} = \begin{bmatrix}1 & 0 & 0 & -1 & 0 & -1\\0 & 1 & 0 & -1 & -1 & 0\\0 & 0 & 1 & 0 & -1 & -1\\0 & 0 & 0 & 4 & 0 & 0\\0 & 0 & 0 & 0 & 4 & 0\\0 & 0 & 0 & 0 & 0 & 4\end{bmatrix}\begin{bmatrix}L_1^2\\L_2^2\\L_3^2\\L_1L_2\\L_2L_3\\L_1L_3\end{bmatrix} \tag{11}$$

In contrast, a convenient linear shape function is proposed for pressure, **such that**

$$\begin{bmatrix}\phi_1\\\phi_2\\\phi_3\end{bmatrix} = \begin{bmatrix}L_1\\L_2\\L_3\end{bmatrix} \tag{12}$$

where $, L_1, L_2$**, and** L_3 **are local triangular coordinates.**

Thus, the mass matrix is given by:

$[T] = 2\pi r_m A[K][M]\,[M^T][K^T]$.

The convective matrices are given by:

$$[Y_r(U_r)] = 2\pi r_m A[K][M][M^T][K^T][U_r][N^T][B^T][K^T],$$

$$[Y_\theta(U_\theta)] = [0],$$

$$[Y_z(U_z)] = 2\pi r_m A[K][M][M^T][K^T][U_z][N^T][C^T][K^T],$$

$$[S_r(U_r)] = 2\pi A[K][M][M^T][K^T][U_r][M^T][K^T],$$

$$[S_\theta(U_\theta)] = -2\pi A[K][M][M^T][K^T][U_\theta][M^T][K^T].$$

The diffusion matrices are given by:

$$[H_r] = 2\pi r_m\, A\frac{1}{Re}[K][B][N][N^T][B^T][K^T],$$

$$[H_\theta] = [0],$$

$$[H_z] = 2\pi r_m\, A\frac{1}{Re}[K][C][N][N^T][C^T][K^T],$$

$$[D_r] = -2\pi A\frac{1}{Re}[K][M][N^T][B^T][K^T],$$

$$[D_\theta] = [0],$$

$$[T_a] = 2\pi\frac{1}{r_m}A\frac{1}{Re}[K][M][M^T][K^T],$$

The gradient matrices are given by:

$$[F_r] = 2\pi r_m A[K][B][N][N^T],$$

$$[F_\theta] = [0],$$

$$[F_z] = 2\pi r_m A[K][C][N][N^T],$$

$$[F_a] = 2\pi A[N][M^T][K^T],$$

such that, A is the area of the triangular element, $r_m = \frac{1}{3}(r_1 + r_2 + r_3)$ **,**

$$[K] = \begin{bmatrix} 1 & 0 & 0 & -1 & 0 & -1 \\ 0 & 1 & 0 & -1 & -1 & 0 \\ 0 & 0 & 1 & 0 & -1 & -1 \\ 0 & 0 & 0 & 4 & 0 & 0 \\ 0 & 0 & 0 & 0 & 4 & 0 \\ 0 & 0 & 0 & 0 & 0 & 4 \end{bmatrix}, \quad [M] = \begin{bmatrix} L_1^2 \\ L_2^2 \\ L_3^2 \\ L_1L_2 \\ L_2L_3 \\ L_1L_3 \end{bmatrix}, \quad [N] = \begin{bmatrix} L_1 \\ L_2 \\ L_3 \end{bmatrix},$$

$$[B] = \frac{1}{2A}\begin{bmatrix} 2\beta_1 & 0 & 0 \\ 0 & 2\beta_2 & 0 \\ 0 & 0 & 2\beta_3 \\ \beta_2 & \beta_1 & 0 \\ 0 & \beta_3 & \beta_2 \\ \beta_3 & 0 & \beta_1 \end{bmatrix}, \qquad [C] = \frac{1}{2A}\begin{bmatrix} 2\gamma_1 & 0 & 0 \\ 0 & 2\gamma_2 & 0 \\ 0 & 0 & 2\gamma_3 \\ \gamma_2 & \gamma_1 & 0 \\ 0 & \gamma_3 & \gamma_2 \\ \gamma_3 & 0 & \gamma_1 \end{bmatrix},$$

such that, βi and γ_j, $i, j = 1,2,3$ are coefficients defined in terms of coordinates of triangular element.

,

Now, by using the Newton-Raphson method to treat the nonlinear part, then by using the backward Euler scheme to treat the time-derivative term, the desired result of these processes is given by:

$$[T][\dot{U}_r] + \left[\frac{\partial R_1}{\partial U_r}\right][\Delta U_r] + \left[\frac{\partial R_1}{\partial U_\theta}\right][\Delta U_\theta] + \left[\frac{\partial R_1}{\partial U_z}\right][\Delta U_z] + \left[\frac{\partial R_1}{\partial P}\right][\Delta P] = -[R_1], \tag{13}$$

$$[T][\dot{U}_\theta] + \left[\frac{\partial R_2}{\partial U_r}\right][\Delta U_r] + \left[\frac{\partial R_2}{\partial U_\theta}\right][\Delta U_\theta] + \left[\frac{\partial R_2}{\partial U_z}\right][\Delta U_z] + \left[\frac{\partial R_2}{\partial P}\right][\Delta P] = -[R_2], \tag{14}$$

$$[T][\dot{U}_z] + \left[\frac{\partial R_3}{\partial U_r}\right][\Delta U_r] + \left[\frac{\partial R_3}{\partial U_\theta}\right][\Delta U_\theta] + \left[\frac{\partial R_3}{\partial U_z}\right][\Delta U_z] + \left[\frac{\partial R_3}{\partial P}\right][\Delta P] = -[R_3], \tag{15}$$

$$[T][\dot{P}] + \left[\frac{\partial R_4}{\partial U_r}\right][\Delta U_r] + \left[\frac{\partial R_4}{\partial U_\theta}\right][\Delta U_\theta] + \left[\frac{\partial R_4}{\partial U_z}\right][\Delta U_z] + \left[\frac{\partial R_4}{\partial P}\right][\Delta P] = -[R_4], \tag{16}$$

where,

$$R_1 = ([Q] + [T_a])[U_r] + [S_\theta(U_\theta)][U_\theta] - \tfrac{1}{Re}[F_r][P],$$

$$R_2 = ([Q] + [T_a] + [S_r(U_r)])[U_\theta],$$

$$R_3 = [Q][U_z] - \frac{1}{Re}[F_z][P],$$

$$R_4 = ([F_r^T] + [F_a])[U_r] + [F_z^T][U_z],$$

such that, $[Q]$ is reduced to the form: $[Q] = [Y_r(U_r)] + [Y_z(U_z)] + [H_r] + [H_z] + [D_r]$.

4. Problem discretization

In this article, the problem of the flow is selected to be a cone connected to upstream and downstream cylinders. In this context, a Poiseuille flow through a 2D-axisymmetric conical channel 1:0.5-cone ($h_1 = 1, h_2 = 0.5$) considered, for an isothermal, incompressible

Newtonian fluid. The radius of the upstream tube is selected to be double of the downstream tube width. Figure 1(a) displayed the schematic diagram of such a benchmark flow problem. Four triangular finite element meshes, M_1, M_2, M_3, and M_4 are used with various half-angles $\alpha = 60^\circ, 45^\circ, 30^\circ, 20^\circ$, respectively, as shown in Figure 1(b). For more details, meshes and angles characteristics are presented in Table 1.

Table 1: Characteristics of the achieved meshes.

Mesh	L_1	L_2	Elements	Nodes Total	Nodes Boundary
M_1	0.3	1	128	297	80
M_2	0.5	1	128	297	80
M_3	0.9	1	128	297	80
M_4	1.4	1	128	297	80

(a)

(b)

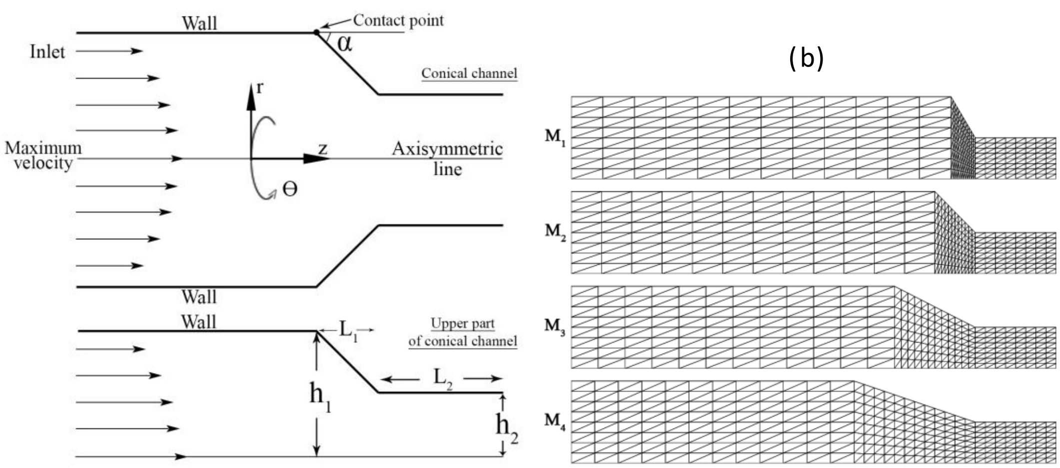

Figure 1: (a) Geometry of the channel, (b) Finite element meshes.

Exact solution: For fully developed shear axisymmetric fluids through a circular upstream channel, the solution in velocity can be computed analytically under specific conditions: steady, incompressible, axisymmetric and laminar flow, with neglected body forces. In this case, for the axis of symmetry $r = 0$ and top wall $r = h_1$, we have the dimensional velocity solution in the form:

$$u_z = (u_z)_{max}\left(1 - \frac{r^2}{h_1^2}\right), \tag{17}$$

where, h_1 is the radius of the channel and $(u_z)_{max}$ is the maximum velocity in the fully developed flow area, which is defined as:

$$(u_z)_{max} = \frac{h_1^2\,\Delta p}{4\mu l} \tag{18}$$

such that, l is the length of the channel and $\Delta p = p_2 - p_1$ where, p_1 and p_2 are the pressure at the outlet and inlet of the channel, respectively.

Boundary conditions (*BCs*): The setting of *BCs* of the present channel problem with $h_1 = 1$ is laid as follows:

1. The inflow conditions are chosen to be those corresponding to the analytical expression (17) for fully-developed axial velocity, and zero radial velocity.
2. A no-slip boundary condition is applied on the top and bottom walls of the channel.
3. Zero radial velocity and zero pressure are applied to the outlet of the channel.
4. Vanished radial velocity along the axisymmetric line.

5. Numerical results

The numerical results are computed for Newtonian flow through the axisymmetric conical channel. In this representation, the study shows tolerance criteria that is taken here as 10^{-6} and typical Δt is $O(10^{-3})$. The findings concerned with the pressure drop and the relationship between the pressure and the Reynolds number (*Re*). In addition, the results concerned with the rate of error convergence of the problem components. Moreover, the effects of some factors, such that the boundary maximum axial velocity and conical half-angle are considered.

History plots of the relative error increment norms in velocity and pressure are illustrated in Figure 2 for Re = 1. Generally, the findings reflect a lower rate of convergence for the pressure compared to that is extracted for velocity under the same rate of time-stepping convergence.

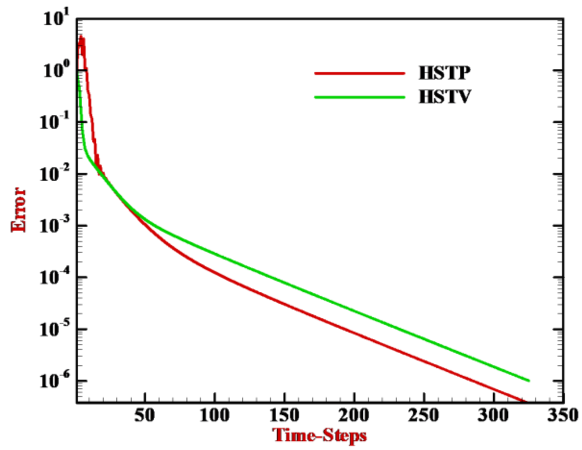

Figure 2: Rate of convergence; Re = 1, M_2 mesh

In Figure 3 fields plot are presented for pressure with Re={0.001, 1, 10, 20}. As to be expected, a maximum level of pressure is displayed at the inlet of the channel, and then decreases gradually by going to the cone exit. Also, the level of pressure rises as Re increases to reach a high level with maxima around 564.072 units with Re = 25.

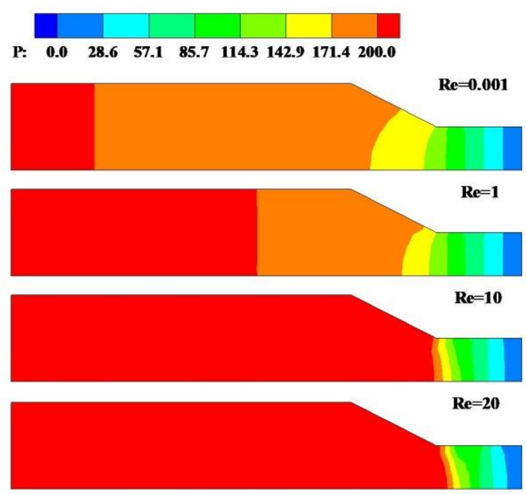

Figure 3: Pressure fields: Re-variation, M_2 mesh.

Pressure drop is plotted in Figure 4(a) with Re= {0.001, 1, 10, 20} along the axis of symmetry. The profiles displayed that there is a significant effect of Re-variation on the pressure distribution over the channel. In this context, the level of pressure drop raised as *Re* increased, reaching a peak of 501.274 with *Re* = 20. Further detail and illustration of this situation, are provided in Figure 4(b), which gives the pressure as a function of *Re*.

(b) (a)

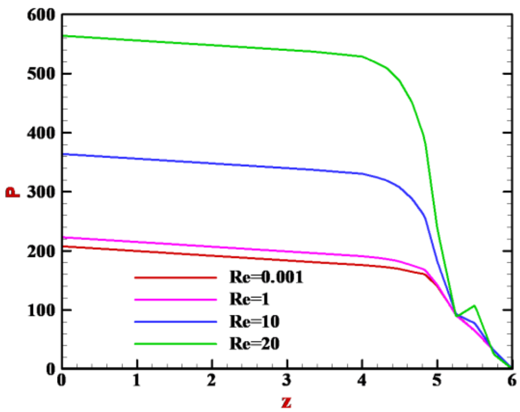

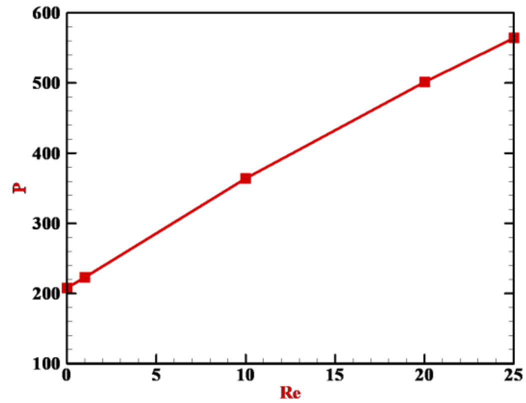

Figure 4: (a) Pressure drop profiles on the axis of symmetry, (b) Pressure as a function of *Re*, M_2 mesh.

The profiles of the axial velocity in fully developed flow at different zones *z* ={2, 4, 5, 6} are presented in Figure 5. The numerical result is provided for *Re* = 1, in two positions; die-section and downstream cone. The axial velocity profiles show parabolic flow structure for both zones, with obviously increasing in the level of velocity whenever we are trending to the cone exit, approaching the maxima of 8 units.

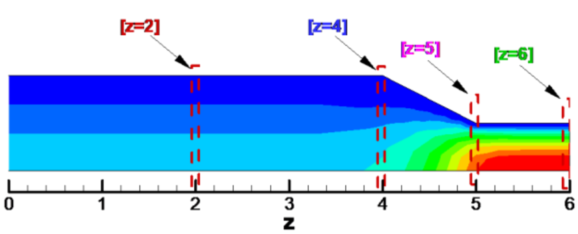

(b) (a)

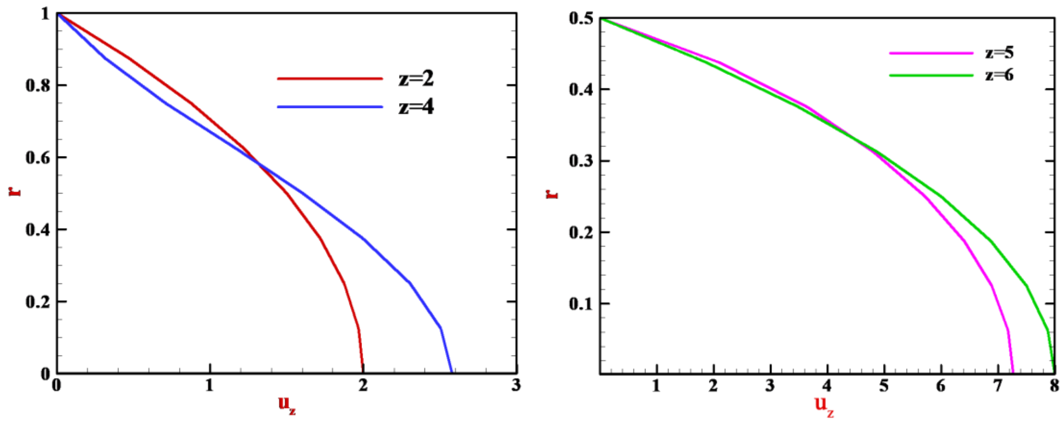

Figure 5: Cross-channel axial velocity profiles, *Re* = 1, M_2 mesh, (a) Die-section, (b) Converging-section.

In addition to the above, the influence of *Re* on the axial velocity along the die-section and downstream cone to the four different *Re* values {0.001, 1, 10, 20} is presented in Figure 6. The results show that, the insignificant effect of *Re*-variation on the axial velocity occurred at the upstream cone, while a notable impact of *Re*-variation appeared at the downstream cone. Generally, one can conclude that, the level of velocity gradually diminished as *Re* increased.

(b) (a)

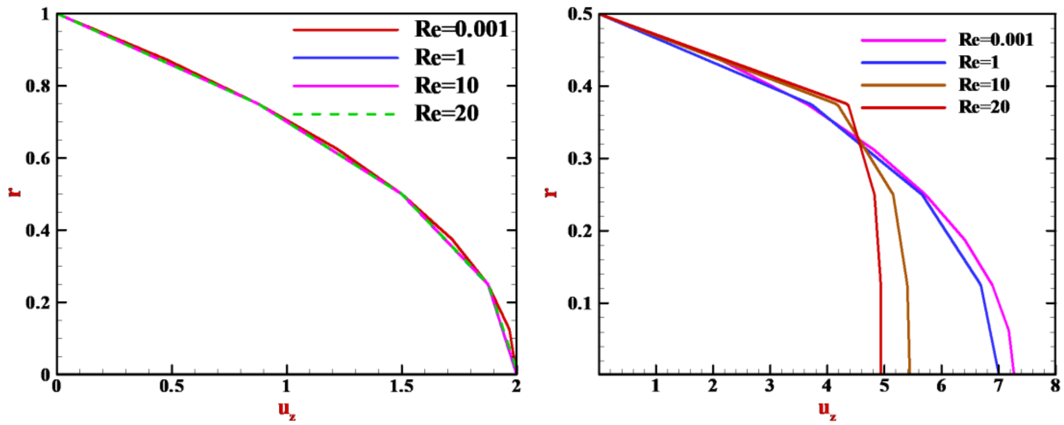

Figure 6: Cross-channel axial velocity profiles, *Re*-variation, M_2 mesh, (a) Die-section at z = 2, (b) Converging-section at z = 5.

Shear data is plotted in Figure 7(a), with shear stress (τ_{rz}) and shear-rate (Γ) along the surface of the cone at four sample *Re* values. The findings reveal that, the peak shear deformation rate (Γ) at *Re* = 20 is 57.94 units near the contact region between the converging section and upstream section; this value decreases to around {48.35, 41.61, 34.46} for *Re* ={10, 5, 1}, respectively. In contrast, there is a change of sign in τ_{rz} is observed compared to Γ, with the least negative level for τ_{rz} is -52.77 units, which is given with the largest *Re* level. In addition, in both cases, a constant level appeared at the die-section, which reflects a pure shear.

In contrast, extensional normal stress (τ_{zz}) and strain-rate (Σ) profiles are shown in Figure 7(b) along the axis of symmetry, corresponding to the same setting of *Re*. The results reflect an opposite feature compared to shear data, where the maximum level of τ_{zz} and Σ occurred with the smallest *Re* level beyond the converging zone. Overall, larger normal stress (τ_{zz}) is noted for *Re* = 1 (of 16.68 units), which is almost two times larger than that for strain-rate (Σ). Here, almost 29% and 31% increase in peak values of τ_{zz} and Σ, respectively, from *Re* = 1 to *Re* = 20.

The effect of $(u_z)_{max}$ that is applied in the inlet of the tube on the level of pressure drop is provided in Figure 8 with fixed *Re*=1. As anticipated, the results illustrated that the level of pressure drop in the inlet of the channel increased as the inlet velocity raised.

(a)

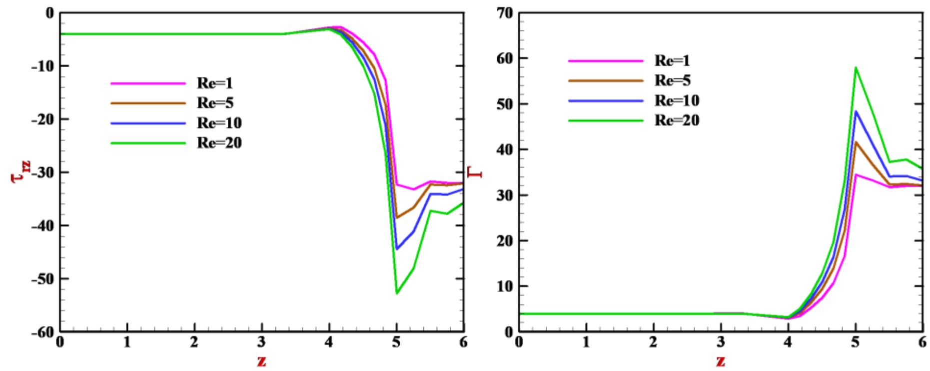

(b)

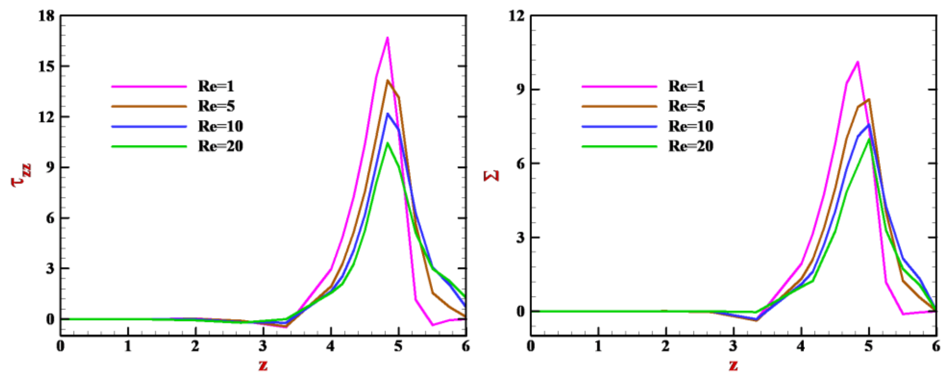

Figure 7: Shear stress (τ_{rz}), shear-rate (Γ), normal stress (τ_{zz}), and strain-rate (Σ); *Re*-variation, M_2 mesh, (a) Along a top wall, (b) Along the axis of symmetry.

The findings of pressure drop give an increasing in pressure values of: *O*(100%) from $(uz)max$ = 1 to $(uz)max$ = 2.

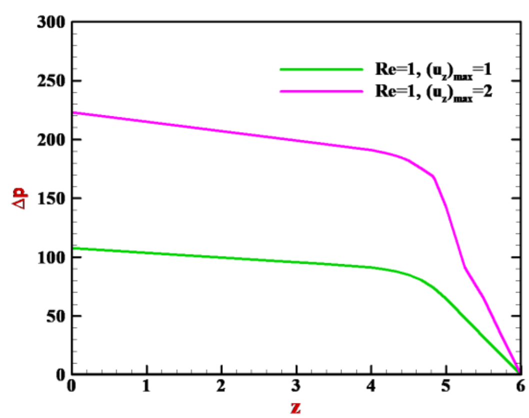

Figure 8: Pressure drop profiles on axis of symmetry; $(u_z)_{max} = \{1,2\}$, $Re = 1$, M_2 mesh.

Effect of conical angle: One of the important results in the current study is the impact of the half-angle for which separation first appears at the cone exit, where the emergence of a recirculation zone will disturb the flow in the cone. To detect the consequence conical half-angle (α) influence on the pressure drop level, the simulation is achieved to the four sample values of angles $\alpha = 60^{\circ}, 45^{\circ}, 30^{\circ}, 20^{\circ}$. For all cases, the pressure drop along the axis of symmetry and the top wall of the conical channel is displayed in Figure 9 for fixed *Re* = 1. The findings reveal that, for both regions, as half-angle levels increase the level of pressure decreases, where maximum value occurs around 234 units with $\alpha = 20^{\circ}$, which is consistent with the results are reported by [11]. In addition, at the top surface of the channel one can observe that the effect of changing the angle on the pressure, where an overshoot in the level of pressure with $\alpha = 45^{\circ}$ occurs (see Figure 9(b)).

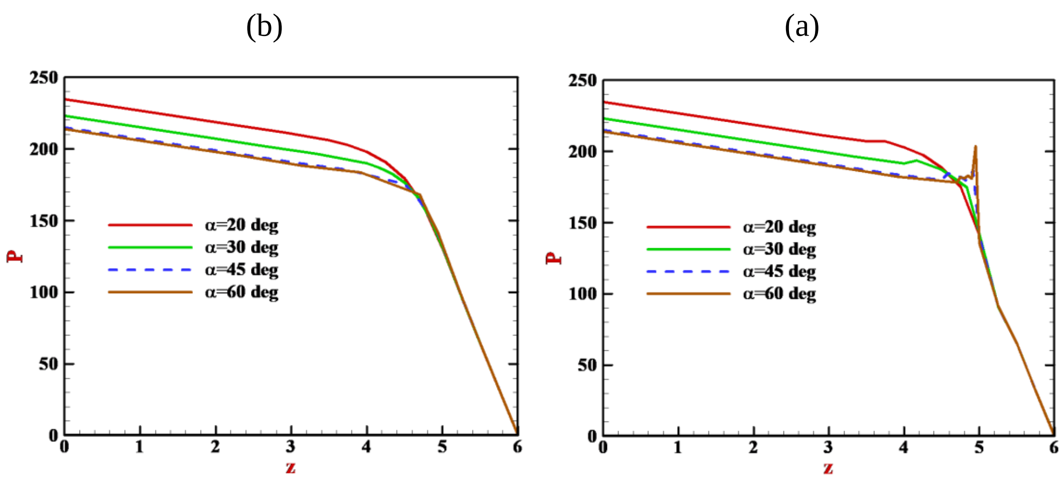

Figure 9: Pressure drop profiles, *Re* = 1, α-variation, (a) Axis of symmetry, (b) Top wall.

Moreover, the impact of varying conical half-angle on the axial velocity at the cone section is presented in Figure 10, for *Re* = 1 and different settings $\alpha = 60^{\circ}, 45^{\circ}, 30^{\circ}, 20^{\circ}$. Here the profiles reflect that, decreasing of the conical half-angle leads to a little increasing of flow velocity level.

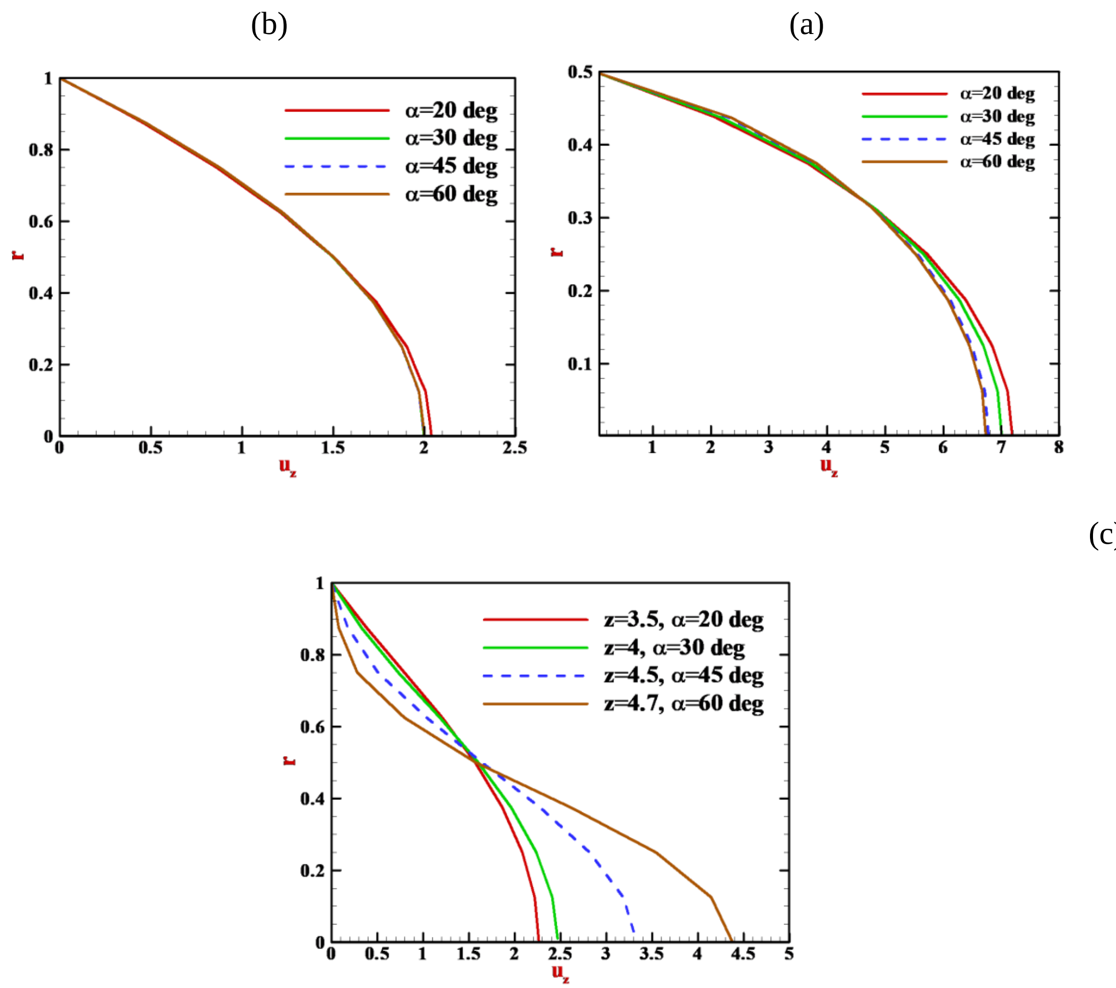

Figure 10: Cross-channel axial velocity profiles; Re = 1, α-variation, (a) Die-section at z = 3, (b) Converging-section at z = 5, (c) Contact point.

The study of the range of shear-rates (Γ) and shear stress (τ_{rz}) can be provided with a complete feature about the deformation history and response of the fluid under consideration. Figure 11 displays the shear-rate (Γ) and shear stress profiles over the top wall for the same settings of α and Re = 1, 5. The constant shear-rate and shear stress levels appeared through the die-section, and then followed by a noticeable increase. The profiles exhibit a modest difference in the levels of shear-rate with variation in conical half-angle (α), reaching a peak value of around 43.49 units with Re = 5 and α = 45°. Similar behavior is observed in τ_{rz} but in the opposite sign, where over the converging section, τ_{rz} increases as α rises. Overall, the shear data reflects that; there is an insignificant effect of α-variation on the shear stress and shear-rate.

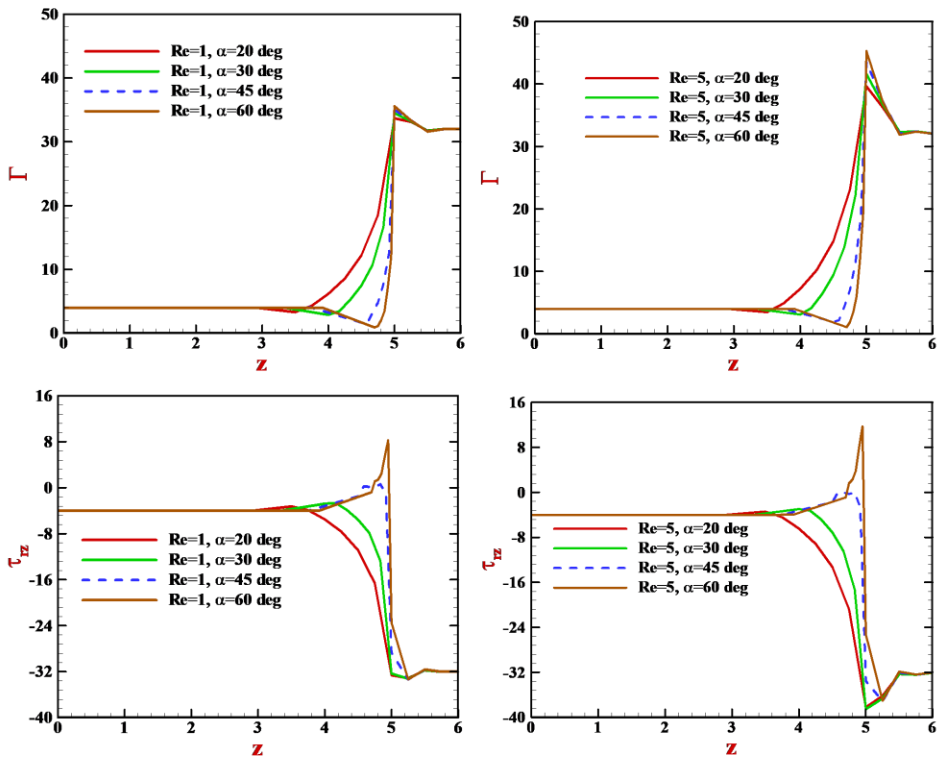

Figure 11: Shear stress (τ_{rz}) and shear-rate (Γ) along a top wall; *Re* = 1,5, *α*-variation, M_2 mesh.

For the same set of parameters, the strain-rate (Σ) and normal stress (τ_{zz}) along the axis of symmetry are provided in Figure 12. Constant normal stress and strain-rate levels occurred along the die-section and cone exit, with an increase and then a sharp decrease over that converging section. From the profiles, one observes an increase in the level of normal stress and strain-rate as *Re* decreases. Also, the results reflect a significant effect of *α* on the peak of extensional stresses, where the maximum level of τ_{zz} and Σ are relevant with a larger angle. Here, the profiles recorded the maximum level of τ_{zz} of around 13.14 units with *Re* = 1 and *α* = 45°. The same trend is observed for Σ, where the peak strain-rate is 20 units at *Re* = 1 and *α* = 45°. Generally, along with the change in the conical half-angle, the value of strain-rate and normal stress will be affected significantly over the converging region.

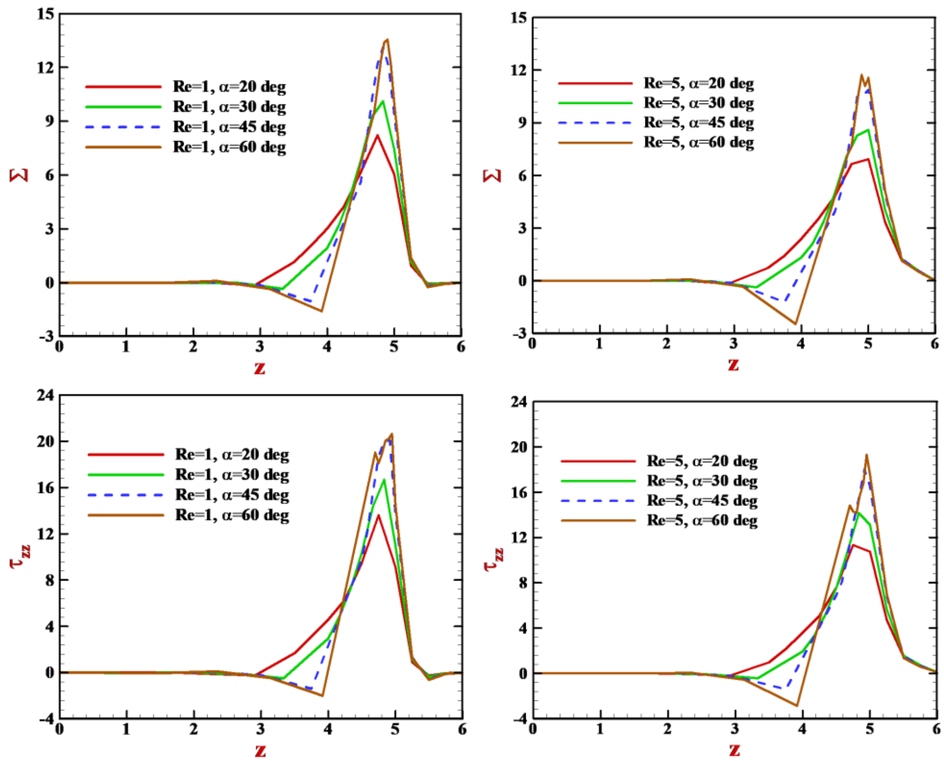

Figure 12: Normal stress (τ_{zz}) and strain-rate (Σ) along the axis of symmetry; Re = 1,5, α-variation, M_2 mesh.

Conclusion

In this study, the numerical simulation for laminar incompressible Newtonian fluid is achieved based on the Galerkin finite element method in the cylindrical coordinates system. With the selected set of parameters, we have commenced with a Reynolds number (Re). The influence of the inlet boundary condition on the behavior of axisymmetric incompressible Newtonian flow is studied as well. The simulation is conducted for four different meshes with various half-angles $\alpha = 60^\circ, 45^\circ, 30^\circ, 20^\circ$. The effect of the boundary maximum axial velocity ($(u_z)_{max}$) at the inlet of the channel on the level of pressure drop is investigated. In this status, we detected that there is a significant effect of $(u_z)_{max}$ upon the level of pressure, such that was generally found that the level of pressure reduces as $(u_z)_{max}$ decreases. In the case of Re, one can see that the maximum Re was around 122 with $(u_z)_{max}$ = 1. Furthermore, the influence of Re-variation on the axial velocity at two regions of the channel; die-section and cone-section is investigated. Ultimately, this study covered the effect of the conical half-angle on the pressure drop levels. Here, the results showed that, the high level of pressure occurred with the small half-angle (α = 20°). The influence of the Reynolds number and conical half-angle on the shear stress, shear-rate, normal stress, and strain-rate is considered. In all cases, a constant response of stresses occurred over the die section, while a notable change in the level of stresses appeared through the converging region. In general, we may pass the comment that; there is a significant effect of *Re* and α on the level of stresses.

References

[1] Z. Cai, B. Lee, and P. Wang, "Least-squares methods for incompressible Newtonian fluid flow: Linear stationary problems," *SIAM Journal on Numerical Analysis*, vol. 42, no. 2, pp. 843–859, 2004.

[2] J. Donea and A. Huerta, *Finite Element Methods for Flow Problems*. West Sussex: John Wiley & Sons, 2003.

[3] P. Kundu, I. Cohen, and D. Dowling, *Fluid Mechanics*, 5th ed. Waltham, MA: Academic Press, 2012.

[4] M. Jalaal, D. D. Ganji, and G. Ahmadi, "Analytical investigation on acceleration motion of a vertically falling spherical particle in incompressible Newtonian media," *Advanced Powder Technology*, vol. 21, no. 3, pp. 298–304, 2010.

[5] D. Lengeler and M. Růžička, "Weak solutions for an incompressible Newtonian fluid interacting with a Koiter type shell," *Archive for Rational Mechanics and Analysis*, vol. 211, no. 1, pp. 205–255, 2014.

[6] K. R. Mahmud, M. M. Rhaman, and A. K. Al Azad, "Numerical simulation and analysis of incompressible Newtonian fluid flows using FreeFem++," *Journal of Advanced Research in Fluid Mechanics and Thermal Sciences*, vol. 26, no. 1, pp. 1–19, 2016.

[7] T. H. Forsyth, "Converging flow of polymers," *Polymer-Plastics Technology and Engineering*, vol. 6, no. 1, pp. 101–131, 1976.

[8] A. B. Jarzebski and W. L. Wilkinson, "Non-isothermal developing flow of a generalised power-law fluid in a tapered tube," *Journal of Non-Newtonian Fluid Mechanics*, vol. 8, pp. 239–248, 1981.

[9] T. H. Kwon, S. F. Shen, and K. K. Wang, "Pressure drop of polymeric melts in conical converging flow: Experiments and predictions," *Polymer Engineering & Science*, vol. 26, no. 3, pp. 214–224, 1986.

[10] S. Oka and A. Takami, "The steady slow motion of a non-Newtonian liquid through a tapered tube," *Japanese Journal of Applied Physics*, vol. 6, no. 4, pp. 423–426, 1967.

[11] G. S. Settles and H. Teng, "Cylindrical and conical flow regimes of three dimensional shock/boundary-layer interactions," *AIAA journal*, vol. 22, no. 2, pp. 194–200, 1984.

[12] J. L. Sutterby, "Laminar converging flow of dilute polymer solutions in conical sections: Part I. viscosity data, new viscosity model, tube flow solution," *AIChE Journal*, vol. 12, 1966.

[13] F. N. Cogswell, "Converging flow and stretching flow: A compilation," *Journal of Non-Newtonian Fluid Mechanics*, vol. 4, no. 1-2, pp. 23–38, 1978.

[14] S. H. Garrioch and D. F. James, "A finite-element study of Newtonian and power-law fluids in conical channel flow," *Journal of Fluids Engineering*, vol. 119, no. 2, pp. 341–346, 1997.

[15] C. Wang, J. Liang, and H. Huo, "Numerical study of effects of geometric parameters on the flow and cavitation characteristics inside conical nozzle of autonomous underwater vehicles," *Advances in Mechanical Engineering*, vol. 11, no. 2, pp. 1–12, 2019.

[16] D. F. James and J. H. Saringer, "Extensional flow of dilute polymer solutions," *Journal of Fluid Mechanics*, vol. 97, no. 4, pp. 655–671, 1980.

[17] G. Ryskin, "Calculation of the effect of polymer additive in a converging flow," *Journal of Fluid Mechanics*, vol. 178, pp. 423–440, 1987.

[18] D. Kwak, C. Kiris, and C. S. Kim, "Computational challenges of viscous incompressible flows," *Computers & Fluids*, vol. 34, no. 3, pp. 283–299, 2005.

[19] R. B. Bird, W. E. Stewart, and E. N. Lightfoot, *Transport Phenomena*, 2nd ed. New York, NY: John Wiley & Sons, 2002.

[20] A. Al-Muslimawi, H. R. Tamaddon-Jahromi, and M. F. Webster, "Numerical simulation of tube-tooling cable-coating with polymer melts," *Korea-Australia Rheology Journal*, vol. 25, no. 4, pp. 197–216, 2013.

[21] A. H. Al-Muslimawi, "Numerical study for differential constitutive equations with polymer melts by using a hybrid finite-element/volume method," *Journal of Computational and Applied Mathematics*, vol. 308, pp. 488–498, 2016.

[22] A. H. Al-Muslimawi, "Taylor Galerkin pressure correction (TGPC) finite element method for incompressible Newtonian cable-coating flows," *Journal of Kufa for Mathematics and Computer*, vol. 5, no. 2, pp. 13–21, 2018.

[23] B. K. Jassim and A. H. Al-Muslimawi, "Numerical analysis of Newtonian flows based on artificial compressibility AC method," *Journal of Al-Qadisiyah for computer science and mathematics*, vol. 9, no. 2, pp. 115–128, 2017.

[24] B. R. Munson, A. P. Rothmayer, T. H. Okiishi, and W. W. Huebsch, *Fundamentals of Fluid Mechanics*, 7th ed. John Wiley & Sons, 2013.

[25] R. Verzicco and P. Orlandi, “A finite-difference scheme for three-dimensional incompressible flows in cylindrical coordinates,” *Journal of Computational Physics*, vol. 123, no. 2, pp. 402–414, 1996.

[26] R. Y. Yasir, A. H. Al-Muslimawi, and B. K. Jassim, “Numerical simulation of non-Newtonian inelastic flows in channel based on artificial compressibility method,” *Journal of Applied and Computational Mechanics*, vol. 6, no. 2, pp. 271–283, 2020.

دراسة عددية لتدفق ممتد خلال بنى هندسية مخروطية متناظرة: طريقة العناصر المنتهية

احمد ناجي عبد الحسن علاء حسن المسلماوي
قسم الرياضيات، كلية العلوم، جامعة البصرة
البصرة، العراق

الخلاصة

في هذه البحث، نقدم دراسة عددية للتدفق الطبقي النيوتوني غير القابل للإنضغاط خلال قناة مخروطية. نحن نطبق طريقة غالركن للعناصر المنتهية لحل المعادلات الحاكمة لمثل هذه المسألة. في العادة، المعادلات الحاكمة للتدفقات النيوتونية غير القابلة للإنضغاط تُمثل بقوانين الحفظ للكتلة والعزم، والتي تُعطى بالإحداثيات الإسطوانية (المتناظرة) في الدراسة الحالية. من المثير للإهتمام، تتم دراسة إنخفاض الضغط خلال القناة تحت قيم متنوعة من عدد رينولدز. الهدف من هذه الدراسة هو تقييم تأثير عوامل مؤثرة مختلفة على مستوى إنخفاض الضغط. بالإضافة لذلك، تأثير السرعة المحورية القصوى الحدودية التي تُفرض في مدخل القناة على الحل يكشف بعض النتائج الجديدة. لتقييم تأثير الزاوية-النصفية المخروطية عند منطقة إعادة الدوران على سلوك الحل، تم اجراء هذه الدراسة لمجموعة مختلفة من الزوايا. لقد وجدنا إن الزاوية-النصفية المخروطية تؤثر بصورة ملحوظة على المستوى الحرج لإنخفاض الضغط. بالإضافة لذلك، إستجابة المائع في الحالتين القصي والممتد تكون مثيرة للإهتمام، والتي تمثل واحدة من الجوانب المهمة لهذه الدراسة.